8379

Assembly and Self-Organization of Silver Nanocrystal Superlattices: Ordered "Soft Spheres"

Brian A. Korgel, Stephen Fullam, Stephen Connolly, and Donald Fitzmaurice*

Department of Chemistry, University College Dublin, Belfield, Dublin 4, Ireland

Received: March 24, 1998; In Final Form: July 29, 1998

Hydrophobic dodecanethiol-capped silver nanocrystals ranging from 50 to 80 Å in diameter were synthesized using arrested growth methods. Size-selective precipitation was employed to isolate nanocrystals homogeneous in size and shape which exhibited close-packed structural order after drying on a carbon or mica substrate. Elemental analysis, H^1 NMR and FTIR spectroscopies were used to characterize the compositional features of the adsorbed thiolate ligands on nanocrystals suspended in solution and condensed in nanocrystal films. Small-angle X-ray scattering (SAXS) and transmission electron microscopy (TEM) were used to probe the structure of both individual nanocrystals and superlattices, and to estimate the energetic interactions between these sterically stabilized particles. In terms of these measurements, the effects of the capping ligand coverage, particle faceting and shape, and interparticle attractions on superlattice formation are elucidated. In particular, the concept of nanocrystals as "soft spheres" which order with an effective hard sphere diameter is introduced. In addition, the ways in which nanocrystals deviate from such an ideal model are discussed.

Introduction

Many technologies—including electronics, health care, separations, and coatings—will be enhanced by the ability to control the structure of materials on a nanometer-length-scale. Furthermore, the unique properties of nanoscale materials may give rise to entirely new technologies. One approach for constructing mesoscopic structures is to use solution-phase nanocrystals as "building blocks".[1−24] Because nanocrystal diameters can range between 20 and 100 Å, these structures would have characteristic dimensions much smaller than those possible using current lithographic technology. One obvious goal for electronic applications is to achieve the capability to position nanocrystals with a high degree of accuracy.

A periodic nanocrystal array, for example, requires the precise positioning of nanocrystals (perhaps on a substrate) with respect to their neighbors. Encouragingly, this architecture is *experimentally* attainable and it has been found that hydrophobic, sterically stabilized nanocrystals can be organized into close-packed arrays simply by evaporating the solvent from a dispersion, provided that the size distribution is sufficiently tight (i.e., a standard deviation about the mean diameter of less than 10%). This general experimental approach to quantum dot superlattice formation has been shown to apply to a variety of materials, such as Au,[17] CdSe,[18,20,24] Ag,[21] Ag_2S,[22] and γ-Fe_2O_3[19] nanocrystals. Up to this point, however, superlattice formation remains highly empirical. Because these arrays could provide the possibility of (1) implementing the unique size-dependent physical properties of individual nanocrystals in a device[17] and (2) eliciting collective electronic and optical properties due to "electronic overlap" resulting from the relative positioning of the nanocrystals in the array,[18,23,24] there is great interest in developing a fundamental understanding of the intrinsic forces that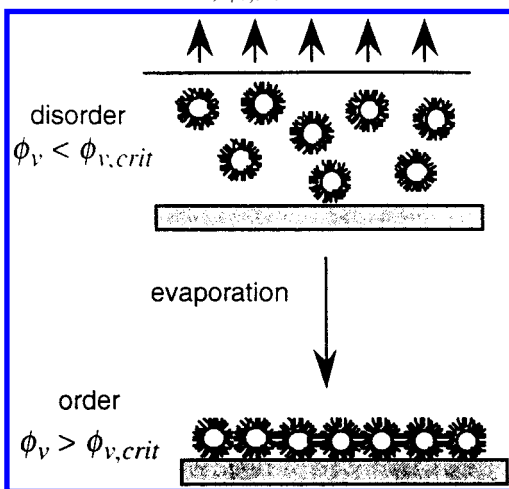 direct superlattice formation. Unquestionably, a deeper understanding will be required in order to increase the complexity of the superlattice structure.

Correctly, it would appear that adequate stabilization and a narrow size distribution are the only requirements for nanocrystal ordering. In 1957, Alder and Wainwright showed using molecular dynamics simulations that size-monodisperse hard spheres (no interparticle attraction when separated) order when particle concentrations exceed a critical volume fraction of 0.49.[25,26] Because the only contribution to the free energy of disorder−order phase transitions for hard spheres is entropy, they have been labeled as entropy-driven phase transitions. As early as 1986, close-packing of "hard sphere" colloids had been confirmed experimentally with size-monodisperse sterically stabilized poly(methyl methacrylate) (PMMA) colloids (∼200−500 nm in diameter).[27] With the application of an external force field (such as solvent convection, gravity, shear flow, or centrifugation) to overcome extremely slow diffusion rates, these large colloids can order into their lowest energy state. Nanocrystals (smaller than 100 Å in diameter), however, diffuse rapidly and can reach local structural equilibrium during solvent evaporation.[28] Therefore, on the basis of experimentally observed ordering of nanocrystal arrays, it appears that the repulsion between particles must dominate the interparticle potential, which in turn would favor entropically driven ordering as high particle volume fractions are reached (Scheme 1).

However, little is known about the interactions between nanocrystals in solution.[29,30] Because these colloidal dispersions are stable for weeks without aggregation, the steric stabilization provided by capping ligands must be sufficient to compensate for the van der Waals (vdW) attraction which would favor particle aggregation. Recently, however, Ohara et al. showed that gold nanocrystals do not behave as expected for hard spheres and that vdW attraction between the nanocrystals considerably affects self-organization during solvent evaporation.[31] Most recently, Korgel and Fitzmaurice showed that the balance between the interparticle attraction and the attraction between particles and the substrate (which can be tuned by

* To whom correspondence should be addressed. Phone: 353-1-706-2441. Fax: 353-1-706-2127. E-mail: dfitz@macollamh.ucd.ie.

8380 *J. Phys. Chem. B, Vol. 102, No. 43, 1998*

Korgel et al.

SCHEME 1: Solvent Evaporation from a Nanocrystal Dispersion on a Substrate: Entropy Drives the Ordering of Hard Spheres When the Particle Volume Fraction Exceeds a Critical Value, $\phi_{v,crit} = 0.49$ [24,25]

Figure 1. (a,b) TEM images of a two-dimensional hcp silver nanocrystal superlattice formed by evaporating a chloroform dispersion on a carbon substrate: $\bar{R} = 34$ and the average minimum interparticle spacing is 15 Å. (c) The 2-D Fourier transform power spectrum of the image in (a).

solvent polarity) determines whether particles form monolayers, bilayers, or multilayers after solvent evaporation.[32] These studies indicate that a purely hard sphere view does not adequately explain nanocrystal self-organization, and that a more detailed understanding of their interactions in solution and how these interactions affect their ordering is needed.

The goals of this report are therefore 2-fold: (1) to provide more detailed structural characterization of dodecanethiol-capped silver nanocrystal superlattices using FTIR and H[1] NMR spectroscopies, transmission electron microscopy (TEM), and small-angle X-ray scattering (SAXS); and (2) to use the findings of this characterization to develop a deeper understanding of the fundamental forces that direct nanocrystal superlattice formation.

Experimental Section

Nanocrystal Synthesis. All chemicals were used as supplied by the Aldrich Chemical Co. and all water was deionized.

Silver nanocrystals smaller than 100 Å in diameter were synthesized at room temperature using a two-phase arrested growth method.[33] Thirty milliliters of an aqueous silver ion solution (0.03 M AgNO$_3$) was combined with 20.4 mL of a chloroformic solution of phase transfer catalyst (0.20 M (C$_8$H$_{17}$)$_4$NBr) and stirred vigorously for 1 h. The organic phase was subsequently collected and 0.16 mg dodecanethiol was added. After the dodecanethiol/Ag$^+$ solution was stirred for 15 min, 24 mL of an aqueous sodium borohydride (0.43 M NaBH$_4$) solution was injected. The reaction mixture was stirred for 12 h before the organic/nanocrystal-rich phase was collected. The dispersion was washed three times with ethanol to remove the phase transfer catalyst, excess thiol, and reaction byproducts. Size selective precipitation using chloroform/ethanol as the solvent/nonsolvent pair was used to narrow the particle size distribution.[3] The isolated dodecanethiol-capped silver nanocrystals redisperse in a variety of organic solvents, such as chloroform, hexane, and toluene.

Characterization Techniques. ^{1}H NMR spectra were recorded using a JEOL JNM-GX270 FT spectrometer at 20 °C. FTIR spectra were recorded using a Mattson Galaxy 3000 FT spectrometer (CaF$_2$ windows, 0.20 mm path length) at 20 °C. TEM was performed using a JEOL JEL-2000 EX electron microscope with a lattice resolution of 0.14 nm and point-to-point resolution of 0.3 nm.
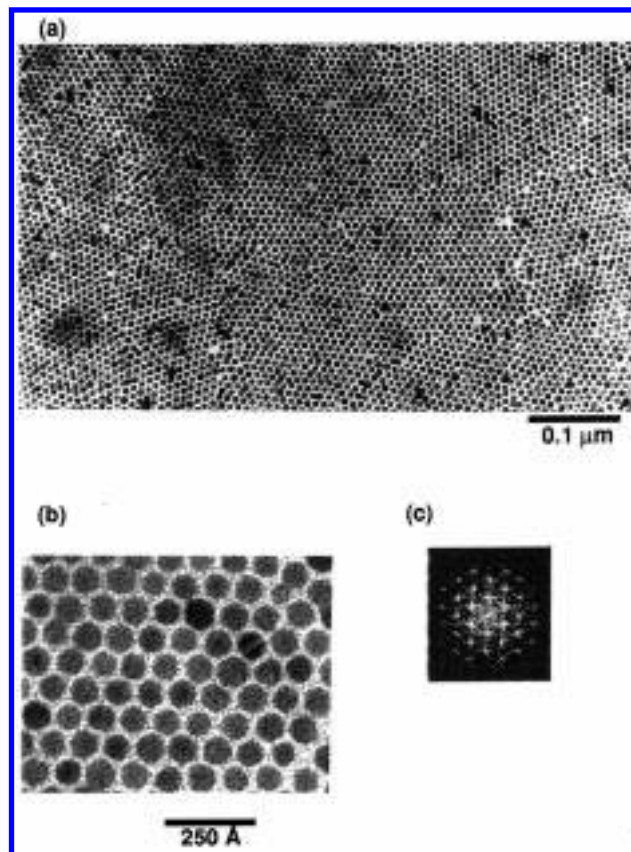
SAXS measurements were obtained using monochromatic radiation of wavelength $\lambda = 1.54$ Å on beam line 8.2 of the Synchrotron Radiation Source (SRS) at the Daresbury Laboratory, Warrington, U.K. Scattered photons were collected on a multiwire gas-filled quadrant detector. The scattering angle was calibrated using an oriented specimen of wet collagen (rat tail tendon). The incident radiation intensity was recorded using a parallel plate ionization detector located before the sample cell. All experimental data were corrected for background scattering, sample absorption, and the positional alinearity of the detector.

Superlattice Formation. Organized arrays of dodecanethiol-capped silver nanocrystals were formed by evaporating the solvent from a dispersion on a substrate at room temperature (20 °C). Dilute dispersions were used to study the interparticle interactions.

Close-packed two-dimensional (2-D) nanocrystal lattices, such as the one shown in Figures 1a and b, were deposited on a carbon-coated copper TEM grid by evaporating approximately 100 μL of a concentrated particle dispersion ($\sim$10^{15} particles/mL chloroform, 0.1% volume fraction). The 2-D Fourier transform power spectra in Figure 1c of the monolayer confirms hexagonal symmetry. Ordered domains in the monolayer typically extend over an area of 0.5 × 0.5 μm in size (approximately 1000 particles). These domains are separated by grain boundaries—apparently as a result of stacking faults. Nanocrystal monolayers such as these can be generated routinely by solvent evaporation to occupy 4.5 μm^2 on a carbon substrate with a point defect frequency (particle vacancies) of 25 μm^{-2}.

Three-dimensional (3-D) superlattices were deposited on mica substrates by evaporating approximately 2 mL of a 7 mg/mL

Ordered "Soft Spheres"

J. Phys. Chem. B, Vol. 102, No. 43, 1998 **8381**

dispersion of nanocrystals in hexane. Small angle X-ray diffraction patterns of these superlattices display sharp diffraction peaks, confirming long range order (see discussion below).

Results and Discussion

"Soft Sphere" Characteristics. The silver nanocrystals generated using the arrested precipitation method described above consist of a silver core coated by adsorbed dodecanethiol ligands which passivate the surface and prevent flocculation in the solvent. Unlike "hard sphere" colloids that exhibit a sharp, infinitely strong repulsion upon touching, these nanocrystals are expected to exhibit a softer, gradually increasing repulsion characteristic of sterically stabilized colloids. Therefore, to determine the magnitude of the steric repulsion, compositional information about the capping ligands is required. ^{1}H NMR and FTIR spectroscopies reveal information about the local molecular environment of the adsorbed thiols, and elemental analysis gives compositional information that correlates with the capping ligand surface coverage.

A comparison of the ^{1}H NMR spectra of dodecanethiol and the dodecanethiol-capped Ag nanocrystals reveals that the α, β, and γ methylene proton resonances from dodecanethiol (δ 2.52, quartet; δ 1.61, quintet; δ 1.31, unresolved multiplet; respectively) broaden after adsorption to the nanocrystals (Figure 2a). (In fact, the α methylene group resonance does not appear in this nanocrystal spectrum.) This line broadening results from both the discontinuity in the diamagnetic susceptibility of the silver−hydrocarbon interface and the residual dipolar interactions in the layer due to spatial constraints, and confirms that dodecanethiol is bound to the particle surface.[34,35] However, the resonances assigned to the C_4−C_{12} methylene protons remain largely unchanged, revealing that the bound ligands extend into the solvent with a relatively high degree of mobility. These resulting molecular motions help provide the steric stabilization necessary to prevent agglomeration in solution.

The FTIR spectra of the nanocrystals provides additional information about the local molecular environment of the thiolate ligands. In Figure 2b, four peaks appear in the FTIR spectra of dodecanethiol. These correspond to the asymmetric and symmetric methylene stretching modes—$\nu_a(CH_2) = 2928$ cm^{-1} and $\nu_s(CH_2) = 2855$ cm^{-1}, respectively—and to the asymmetric in-plane and symmetric stretching modes of the terminal methyl groups—$\nu_a(CH_3,ip) = 2954.5$ cm^{-1} and $\nu_s(CH_3,$-FR$) = 2871$ cm^{-1}, respectively.[36] These peak maxima are shifted to slightly lower wavenumbers in the nanocrystal spectra—$\nu_a(CH_2)$ shifts from 2928 to 2926.5 cm^{-1} and $\nu_s(CH_2)$ shifts from 2855 cm^{-1} to 2854 cm^{-1}, respectively—suggesting that the thiolate molecular motions are somewhat constrained, presumably because of the formation of a relatively close-packed thiol layer on the nanocrystal surface.[36] Nonetheless, these are relatively small shifts—compared to $\Delta\nu_a(CH_2) \approx 10$ cm^{-1} and $\Delta\nu_s(CH_2) \approx 5$ cm^{-1} typically measured for self-assembled monolayers (SAMs) of alkanethiols on flat gold and silver substrates—which indicates an essentially liquidlike adsorbed alkyl layer, consistent with the ^{1}H NMR data in Figure 2a.[37]

To ensure that the liquidlike nature of the capping ligands is not simply due to poor surface coverage, elemental analysis was used to measure the ratio of silver and organic molecular masses which could be used to calculate explicitly the capping ligand surface coverage using the average particle radii determined from TEM and/or SAXS.[37] Assuming spherical particles, we calculated the thiol "footprint" (averaged for six different preparations) to be 16 ± 2 Å^2/thiol. Particle sizes ranging in diameter from 40 to 75 Å were examined, and the thiolate
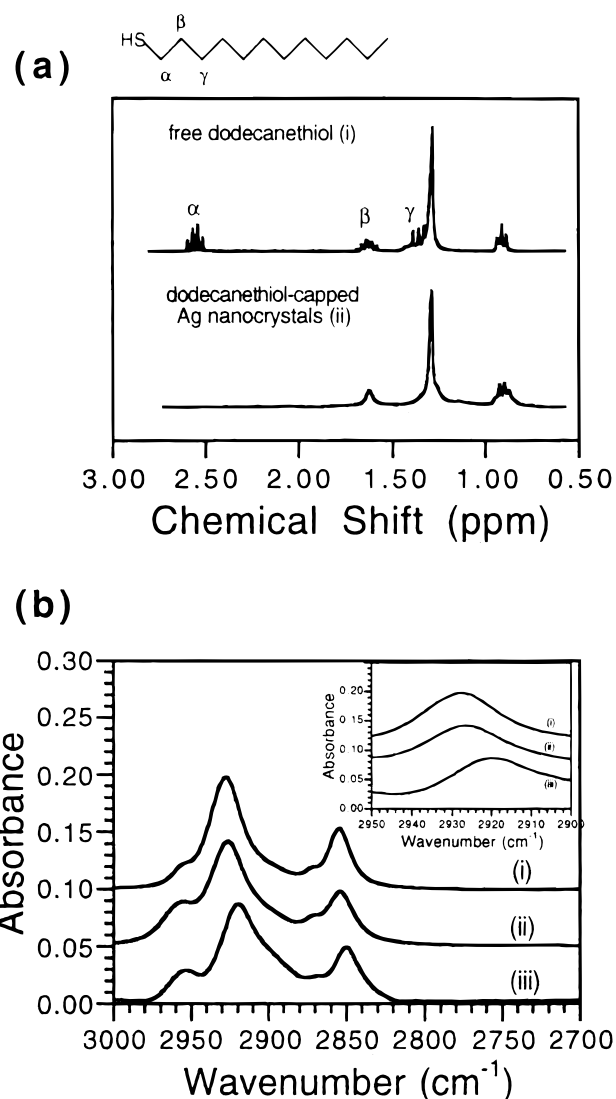

(a)

(b)

Figure 2. (a) ^{1}H NMR and (b) FTIR spectra: (i) free dodecanethiol in chloroform-*d*; (ii) dodecanethiol-capped Ag nanocrystals in chloroform-*d*; (iii) silver nanocrystal superlattice on a CaF$_2$ window. Inset (b): expansion of the $\nu_a(CH_2)$ peak maxima—(i) 2928 cm^{-1}; (ii) 2926.5 cm^{-1}; (iii) 2919.5 cm^{-1}.

surface coverage did not appear to correlate with the nanocrystal diameter. When a shell approximation is used to calculate the number of silver atoms exposed on a nanocrystal surface, thiols bind with a surface coverage of $75 \pm 10\%$ (with 95% confidence).[39]

The measured value of 16 ± 2 Å^2/thiol on the nanocrystals is significantly less than the value of 21.4 Å^2/thiol[40−42] measured for SAMs on flat gold surfaces. (The corresponding separation distance of 4.3 Å between thiols on the nanocrystal surface is nonetheless greater than the theoretical physical limit of 4.2 Å.[41]) However, consider that the adsorbed alkylthiolate radiates from the particle surface and that the intermolecular spacing increases rapidly as a function of radial distance due to the extreme curvature of the nanocrystal surface. When a thiol molecular length of 15 Å[37] is used, the area occupied by the thiol on a 70 Å diameter nanocrystal increases from 16 Å^2/thiol to 32.7 Å^2/thiol at the end of the alkyl chain. Therefore, the liquidlike structure of the adsorbed thiol layer does not result from poor surface coverage, but rather from the extreme curvature of the nanocrystal surface.

With knowledge of the thiol coverage on the nanocrystal surface, the energy of the steric repulsion between two dode-
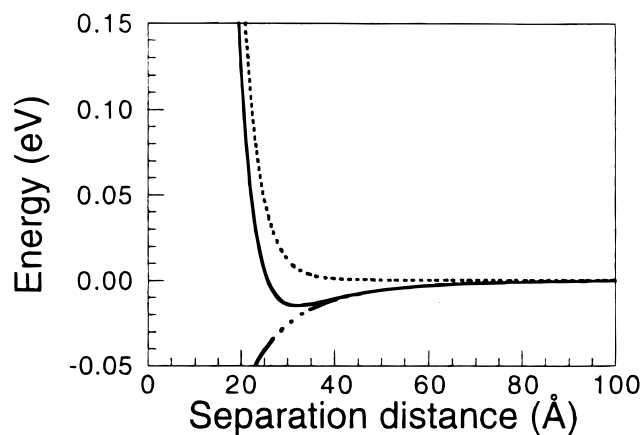
Figure 3. Interparticle potential (—) between two dodecanethiol-capped 70 Å diameter silver nanocrystals: (- - -) E_{steric} plotted using (1); (—) E_{vdW} plotted using (2) as described in the text.

canethiol-capped silver nanocrystals can be calculated explicitly using the expression derived by de Gennes for two dense layers of strongly adsorbed chains in a good solvent,[42]

$$E_{steric} \approx \frac{100 \, R\delta_{SAM}^2}{(C-2R)\pi\sigma_{thiol}^3} kT \exp\left(\frac{-\pi(C-2R)}{\delta_{SAM}}\right) \quad (1)$$

where δ_{SAM} is the brush thickness (15 Å),[37] and σ_{thiol} is the diameter of the area occupied by the thiol on the particle surface (4.3 Å). The interparticle interaction potential also includes the long range vdW attraction, which is relatively strong between these nanocrystals because of the large polarizability of the silver cores. Using the expression derived by Hamaker,[45]

$$E_{vdW} = -\frac{A}{12}\left\{\frac{4\,R^2}{C^2-4\,R^2} + \frac{4\,R^2}{C^2} + 2\ln\left[\frac{C^2-4\,R^2}{C^2}\right]\right\} \quad (2)$$

where A is the Hamaker constant and C is the center-to-center distance between spheres; the interaction potential ($E_{vdW} + E_{steric}$) between two dodecanethiol-capped 70 Å silver nanocrystals can be calculated. Taking $A = 1.95$ eV for silver–silver attractions across a hydrocarbon layer,[46] Figure 3 shows that a weak attractive energy minimum of approximately 1/2 kT exists before a steeply increasing repulsion dominates the potential at separations less than 18 Å. This repulsion provides the entropic freedom between nanocrystals necessary for ordering to occur. Therefore, analogous to hard spheres, these soft sphere nanocrystals have an effective radius, R_{eff}, that extends 9 Å beyond the silver core radius.

Evaporation of a chloroform dispersion of size-monodisperse dodecanethiol-capped silver nanocrystals on a carbon substrate yields a nanocrystal monolayer as shown in Figure 1a (provided that the substrate loading is less than one monolayer). The adsorbed long-chain alkanethiol molecules maintain the separation between silver cores after solvent removal with a characteristic interparticle spacing, or effective soft sphere radius. The narrow particle size distribution allows the particles to order into a planar hexagonal close-packed (hcp) array. However, if these were hard silver cores ordering in the monolayer, they would be below the critical volume fraction ($\phi_v = 0.59 < \phi_{v,crit} = 0.63$) for the disorder–order phase transition calculated for two-dimensional disks.[26] Therefore, the nanocrystals order as if they were hard spheres with an effective particle diameter that includes the corona of the organic coating.

To confirm such soft sphere behavior, SAXS was used to obtain more statistically representative (or at least complementary) average nanocrystal sizes, size distributions, and superlattice structures.

The intensity of radiation scattered by a dispersion of particles, $I(\theta)$, can be expressed as a function of the scatterer electron density, ρ_e, the shape factor, $P(\theta)$, and an interparticle scattering factor, $S(\theta)$:[47]

$$I(\theta) = \rho P(\theta) S(\theta) \quad (3)$$

(In eq 3, ρ is a constant proportional to ρ_e). Because the electron density of the thiolate ligands does not significantly differ from the solvent, the measured scattering intensity results from the silver nanocrystal core alone. For noninteracting particles, $S(\theta) = 1$, and the average particle diameter in a dispersion can be determined from the shape of the scattering curves using analytical expressions for $P(\theta)$. For an isotropic sphere,[47,48]

$$P(\theta) = P(qR) = \left[3\frac{\sin(qR) - qR\cos(qR)}{(qR)^3}\right]^2 \quad (4)$$

The wave vector, q, is defined as $q = (4\pi/\lambda)\sin(\theta)$, where θ is the scattering angle 2θ. It is apparent that q is inversely proportional to the characteristic d spacing in the system: $d = 2\pi/q$. For a polydisperse sample, the size distribution, $n(R)/n_{total}$, affects $I(\theta)$:[47,48]

$$I(q) \propto \int_0^\infty \left(\frac{n(R)}{n_{total}}\right) P(qR) R^6 \, dR \quad (5)$$

To calculate the average particle radius, $\bar{R}$, and the standard deviation, σ, from the SAXS data, the shape of the size distribution must be assumed. Therefore, a Gaussian distribution, where

$$\frac{n(R)}{n_{total}} = \frac{1}{\sigma\sqrt{2\pi}} \exp\left[\frac{-(R-\bar{R})^2}{2\sigma^2}\right] \quad (6)$$

was assumed for the curve fits in Figures 4 and 5a.

Figures 4 and 5a show typical scattering data for dodecanethiol-capped silver nanocrystals dispersed in hexane. The scattering intensity oscillates with q. Breadth in the particle size distribution damps the oscillations at higher scattering angles. In Figure 4a, four oscillations are evident, which indicates a relatively tight size distribution. Replotting the data as Iq^4 vs. q (a Porod plot) further enhances the oscillations in the scattering data (Figure 4b). Again, damping of the oscillations as q increases results from the presence of a distribution of particle sizes. Fitting the data using (4), (5), and (6) yields $R = 35.0 \pm 2.7$ Å. The effect of the beam width at lower q produces a deviation between the data and the curve fit, particularly evident in Figure 4a in the first two curve minima.[47] The inset in Figure 4b shows that the q-value of the measured peak maxima and peak minima of Iq^4 agree with the positions predicted by the model curve (indicating that $\bar{R}$ is accurate). The damping of Iq^4 in Figure 4b is also represented well by the curve fit (indicating that σ is accurate). The histogram in the inset in Figure 4a determined for these nanocrystals by counting 500 particles in a TEM image gave $R = 34.0 \pm 2.5$ Å. The difference between the values measured using TEM and SAXS is within experimental error.

Figure 5 shows SAXS measurements for three different nanocrystal samples collected after consecutive size-selective precipitations. Figure 5a shows the data and curve fits for the
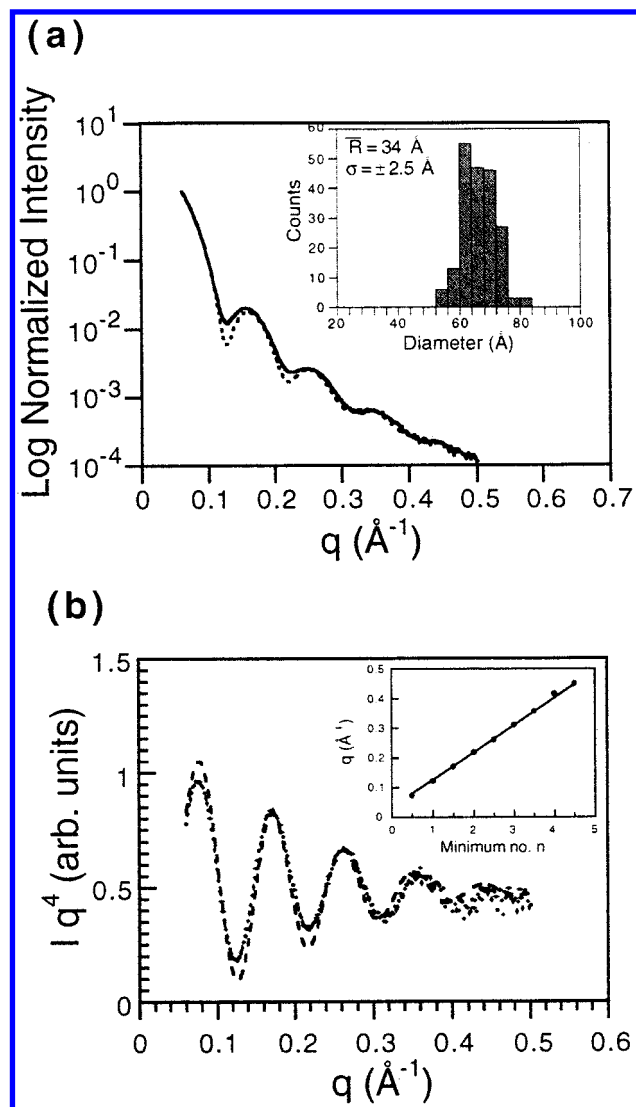
Ordered "Soft Spheres"

J. Phys. Chem. B, Vol. 102, No. 43, 1998 **8383**

Figure 4. (a) Small-angle X-ray scattering data of dodecanethiol-capped silver nanocrystals dispersed in hexane (7 mg/mL, third fraction in Figure 5). (b) Porod plot of the data in (a). The curves (- - -) in (a) and (b) represent the best fit of (4), (5), and (6) to the data as discussed in the text: $R = 35 \pm 2.7$ Å. Inset in (a): histogram constructed by sizing 500 nanocrystals using TEM. Inset in (b): (●) q at the peak maxima and minima in the Porod plot compared to the curve fit (—).

samples dispersed in hexane. A single precipitation isolates particles differing by approximately one lattice plane width in radius, with standard deviations of approximately $\sigma \approx \pm 8\%$: (i) $R = 39.0 \pm 3.6$ Å; (ii) $R = 38.0 \pm 3.0$ Å; (iii) $R = 35.0 \pm 2.7$ Å.

Spin coating a mica substrate with one of these dispersions yields a thin violet transparent residue which scatters X-rays as shown in Figure 5b. Indexing the patterns reveals face-center cubic (fcc) superlattice structure with lattice constants that correlate with the average particle radii determined in Figure 5a. These data also suggest that the (111) superlattice planes lie perpendicular to the substrate normal, indicating that the hcp monolayers observed at low particle loading form the basal plane of more extended superlattices, which build up from the substrate as the solvent evaporates.

The center-to-center distances between nanocrystals, C, in the fcc supercrystals in Figure 5b were computed from the d_{111}-spacing: $C = d_{111}/\cos 30°$. The interparticle spacing, δ_{SL}, results from the presence of the capping ligands and can be
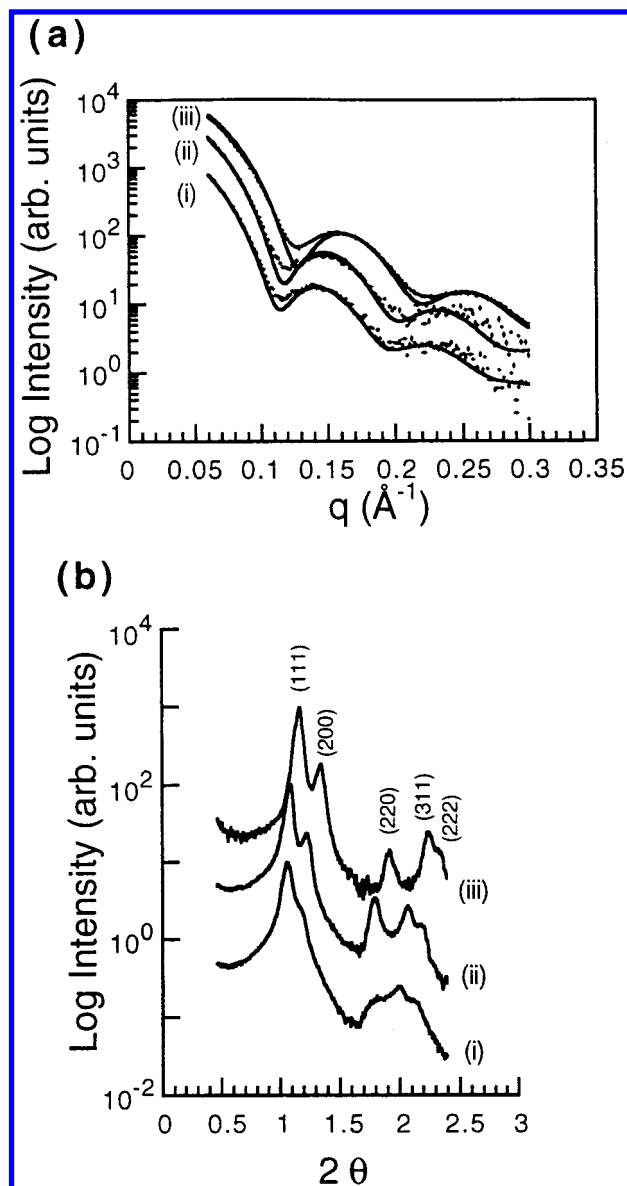

Figure 5. Small-angle X-ray scattering of dodecanethiol-capped silver nanocrystals (a) dispersed in hexane (5−7 mg/mL) and (b) crystallized on a mica substrate for three consecutive fractions—(i), (ii), (iii, sample in Figure 4)—collected after size selective precipitation. The curve fits in (a) represent the best fit of (4), (5), and (6) as described in the text: (i) $R = 39 \pm 3.6$ Å; (ii) $R = 38 \pm 3.0$ Å; (iii) $R = 35 \pm 2.7$ Å. The diffraction patterns in (b) index to fcc structure with d_{111} spacings of (i) 83 Å, (ii) 82 Å, and (iii) 76 Å.

computed from C: $\delta_{SL} = C - 2\bar{R}$. From the values of d_{111} determined from Figure 5b and $\bar{R}$ determined from Figure 5a, δ_{SL} was computed to be (i) 17 Å; (ii) 18.5 Å; and (iii) 17.5 Å. This is within experimental error of the value determined for sample (iii) using TEM: $\delta_{SL} = 16$ Å. For the samples shown in the TEM images in Figures 1 and 6, δ_{SL} is 15 and 19 Å, respectively. Therefore, for this size range, there is no apparent trend in the particle size dependence of δ_{SL}. Averaging the values obtained using SAXS and TEM for the dodecanethiol-capped silver nanocrystal superlattices studied, the average value for δ_{SL}, $\bar{\delta}_{SL}$, was found to be 17 Å—significantly less than twice the thickness of a dodecanethiol SAM on a flat substrate.[37] Others have observed compressed interparticle spacing as well and have proposed either chain interdigitation or chain folding to explain this phenomenon.[21,34,35]

From the interparticle spacing determined using TEM and SAXS, the organic molecular density in the superlattice is
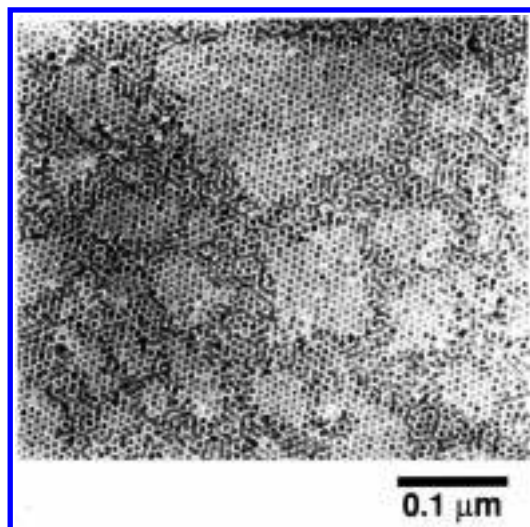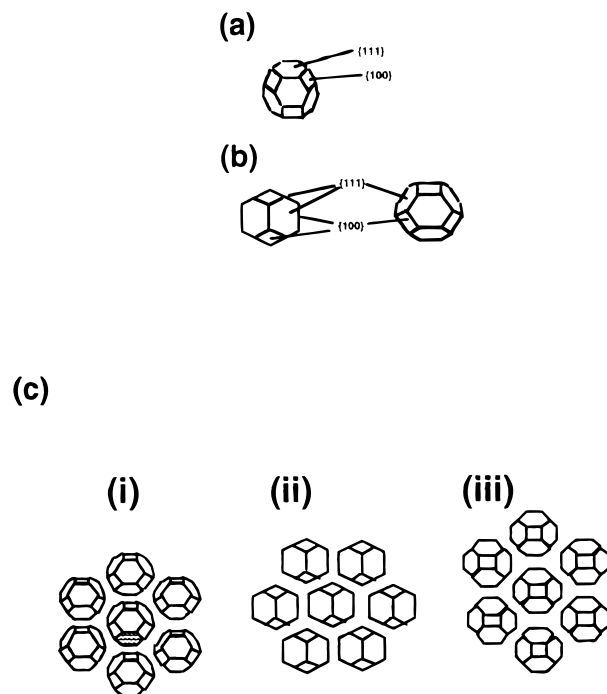
Figure 6. TEM image of 45 Å diameter dodecanethiol-capped silver nanocrystals evaporated from a chloroform dispersion onto a carbon substrate at a surface loading slightly higher than that needed for a close-packed monolayer. The positioning of the particles in the second layer is evident. The average minimum interparticle spacing is 19 Å.

SCHEME 2: A Truncated Icosahedron is the Wigner–Seitz Cell for a Particle with an fcc Core Structure: (a) Perspective and (b) Top Views.[50] (c) Top View of a Nanocrystal Monolayer with Three Hypothetical Nanocrystal Orientations: (i) the {111} Plane Flush with the Substrate; (ii) Lying on the Edge Separating the {111} Planes; (iii) the {100} Plane Flush with Substrate[a]


[a] Maximization of the van der Waals attraction between particles and the substrate favors (ii), as discussed in the text.

readily calculable and can be compared to the chain density of dodecanethiol in SAMs on flat substrates. Taking the measured value of a_{thiol}, the surface of a spherical 70 Å diameter silver nanocrystal would carry 920 thiol ligands. With an interparticle spacing of 17 Å in an fcc superlattice, the specific volume of dodecanethiol in the interstitial space is 300 Å^3/thiol. This agrees very well with that measured for dodecanethiol adsorbed to flat gold surfaces (∼314 Å^3/thiol)[36] and implies that the chain flexibility enables complete space filling in the nanocrystal array. The FTIR spectrum of the nanocrystal superlattice further indicates a high capping ligand density. The methyl and methylene absorbance peaks in Figure 2b shift to lower wavenumbers in the superlattice and ν_a(CH$_2$) and ν_s(CH$_2$) match those found for thiolate SAMs packed on flat substrates (see caption to Figure 2b for values).[37] Although ligand tangling surely occurs in the superlattice due to the flexibility of the ligands, Corey–Pauling–Koltun space-filling models suggest that the close-packed thiol groups on the particle surface do not allow the hydrocarbons to fully extend at the minimum interparticle separation. On this basis, it is concluded that the thiolate *density* and not chain length controls the interparticle spacing.

Similar to the hcp nanocrystal monolayers discussed above, the silver core volume fraction in the 3-D superlattice is only 0.40, significantly below that required for a disorder–order phase transition for hard spheres (0.49).[26] As a consequence, it was suggested that these nanocrystals behave as soft spheres with effective radii that include at least part of the capping layer thickness. Further supporting this view, the interparticle spacing measured for superlattices of 70 Å diameter dodecanethiol-capped silver nanocrystals using SAXS corresponds closely to the interparticle separation at which point the interaction potential becomes infinitely repulsive. This is consistent with findings for diblock copolymer micelles in which the "corona" that surrounds the particle "core" contributes to the critical volume fraction measured when ordering of these spheres occurs.[49]

Therefore, the formation of ordered close-packed nanocrystal arrays requires both a narrow core size distribution and consistent capping ligand surface coverage throughout the sample. Because the capping ligands contribute to R_{eff}, broad deviations in the surface coverage would eliminate the nano-

crystal disorder–order phase transition and superlattice formation would not occur.

Deviations from Soft Sphere Behavior. Because the silver nanocrystals are in fact rigid metallic cores surrounded by soft capping ligands, it might be expected that the core structure can in some cases affect the ordering of the particles. Furthermore, the attraction between particles, although relatively small, might also affect nanocrystal self-assembly.

The shape of the silver nanocrystal core can vary significantly within a single preparation, with particles ranging from spheres, to faceted spheres, to ellipsoids with aspect ratios up to 1.4. However, provided that the initial shape distribution is reasonably tight, size selective precipitation can isolate particles with a particular shape as well as size. The particle shape subsequently leads to ordered phases that differ substantially from those expected for nanocrystals that behave as soft spheres.

(i) Faceted Nanocrystals. Faceting of the silver core affects the nanocrystal orientation in a monolayer. (Obviously, faceted nanocrystals are not geometrically isotropic like spheres, and deviations from soft sphere packing will certainly appear if the silver cores "feel" each other.) Most of the dodecanethiol-capped Ag nanocrystals shown in Figure 1b exhibit six edges. These faceted nanocrystals are representative of all faceted spheroidal nanocrystals prepared under the conditions reported. The facets in this monolayer are in registry. Presumably, these faceted nanocrystals form truncated icosahedra—the Wigner–Seitz cell for a particle with an fcc core structure (such as silver)—as shown in Scheme 2, where the {100} and {111} silver planes form the facets.[50] Depending on the particle orientation on the substrate, a TEM image of a truncated

Ordered "Soft Spheres"

J. Phys. Chem. B, Vol. 102, No. 43, 1998 **8385**

SCHEME 3: Hypothetical Constructions of Particles Forming a Partial Bilayer at High Substrate Loading[a]
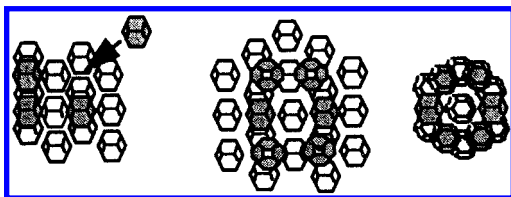
[a] Notice the effect of nanocrystal faceting on the order perpendicular to the substrate.

icosahedra could reveal six, eight, or possibly zero distinct facets (positions (ii), (iii), (i), in Scheme 2c, respectively). Six facets would be evident in a TEM image only when the silver nanocrystal lies on the edge separating the {111} planes (position (ii) in Scheme 2c) and for no other orientation. Such an orientation is largely due to the maximization of the vdW interactions between the facets of neighboring nanocrystals (as depicted in position (ii) in Scheme 2c).[51] At short separation distances, the attractive energy between two nanocrystal edges (approximately that of two spheres) is inversely proportional to the separation distance—$E_{edges} \overset{\sim}{\propto} 1/\bar{\delta}_{SL}$—whereas, between two flat surfaces, $E_{facets} \overset{\sim}{\propto} 1/(\bar{\delta}_{SL})^2$.[45] Therefore, each particle energetically favors an orientation that maximizes the number of aligned planes. The orientation (ii) in Scheme 2c, in which six nanocrystal facets align with six other {111} nanocrystal facets, maximizes the vdW interactions between the silver cores despite the less favorable interaction of the nanocrystal edge with the substrate.

The interaction between particle facets also affects the positioning of nanocrystals that adsorb on top of a fully developed monolayer, as shown in the TEM image in Figure 6. Instead of settling into the entropically favored (for hard spheres) position in the trough centered between three particles in the bottom layer, a large proportion of the add-particles bridges two monolayer particles because of the vdW attraction between silver cores. Scheme 3 depicts a number of possible orientations sensitive to faceting and the surface-shape-dependent vdW attractions between particles (facets). At higher loadings, however, SAXS reveals that the nanocrystal layers close pack into extended fcc structures as would be expected for soft spheres (Figure 5b). These results emphasize the cooperativity that occurs in this self-assembling and self-organizing system. At high-volume fractions, the interactions between all of the nanocrystals (both those already adsorbed on the substrate and those in solution) determine the nanocrystal location in the superlattice. In contrast, at low volume fractions the local interactions with the nanocrystals in the bottom monolayer determine the particle orientation.

(ii) Interparticle Attraction. The net attractive energy between particles because of vdW forces is particularly evident in dilute submonolayers where the attraction between nanocrystals produces an unusually high degree of interparticle sticking. For example, in the TEM image of a substrate with a very dilute substrate loading (0.01 mg/mL) shown in Figure 7a, 50% of the particles have formed dimers or multimers with triangular structures. Figure 7b (0.1 mg/mL) shows a substrate with slightly higher loading in which a large proportion of the nanocrystals have aggregated into larger clusters of particles. The nanocrystals in these clusters—with as few as 12 particles— have organized into regular 2-D structures indicating that the interparticle interactions are reversible with characteristic energy on the order of kT. These particle volume fractions (considering nanocrystals as soft spheres with R_{eff}) are much too low to
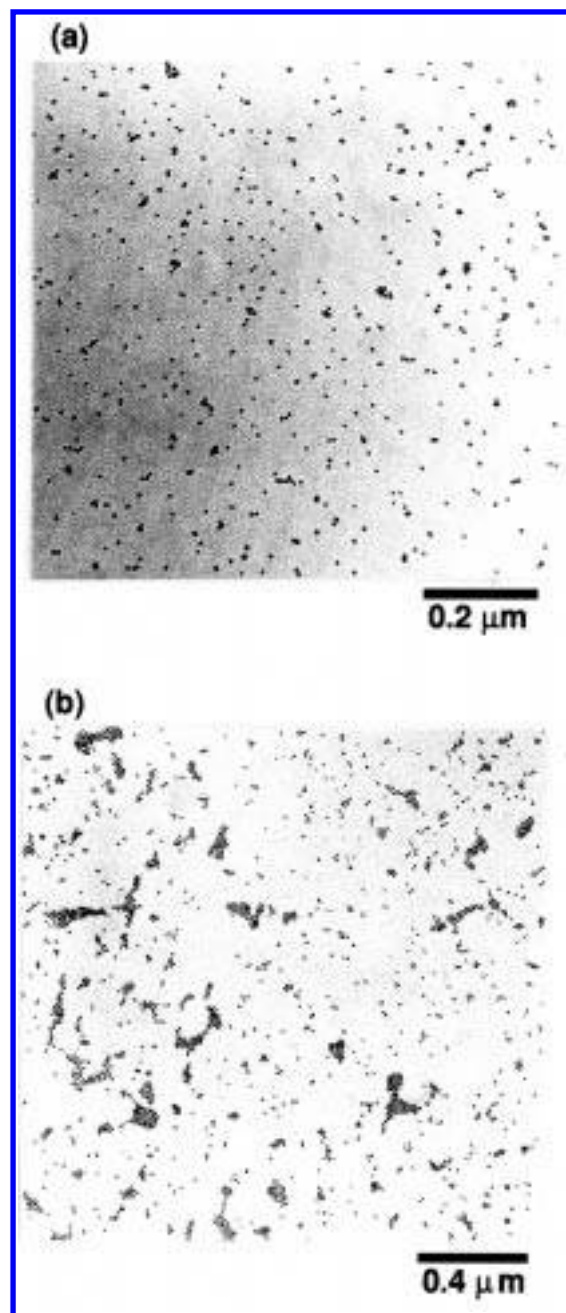

Figure 7. TEM images of dilute suspensions of 70 Å diameter dodecanethiol-capped silver nanocrystals evaporated on a carbon substrate. Despite the low concentration, particularly in (a), a large proportion of particles form dimers and multimers. Interparticle interactions, however, are not sufficiently strong to induce fractal formation and aggregates consisting of as few as 14 nanocrystals display ordering as shown in (b).

induce entropically driven ordering; therefore, these results indicate that the interparticle attraction helps position the nanocrystals in the monolayer to achieve ordering.[52]

The attractions between nanocrystals in very dilute dispersions are evident in SAXS measurements as well. Figure 8a shows the X-ray scattering behavior of dilute dispersions of sample (iii) (from Figures 4 and 5) in hexane with decreasing particle concentration. The distance distribution function, $p(r)$,[53]

$$p(r) = \frac{1}{2\pi^2} \int_0^\infty I(q) qr \sin(qr) \, dq \tag{7}$$

of the most concentrated sample in Figure 8a behaves as expected for hard spheres with $R = 35$ Å (Figure 8b). (Compare
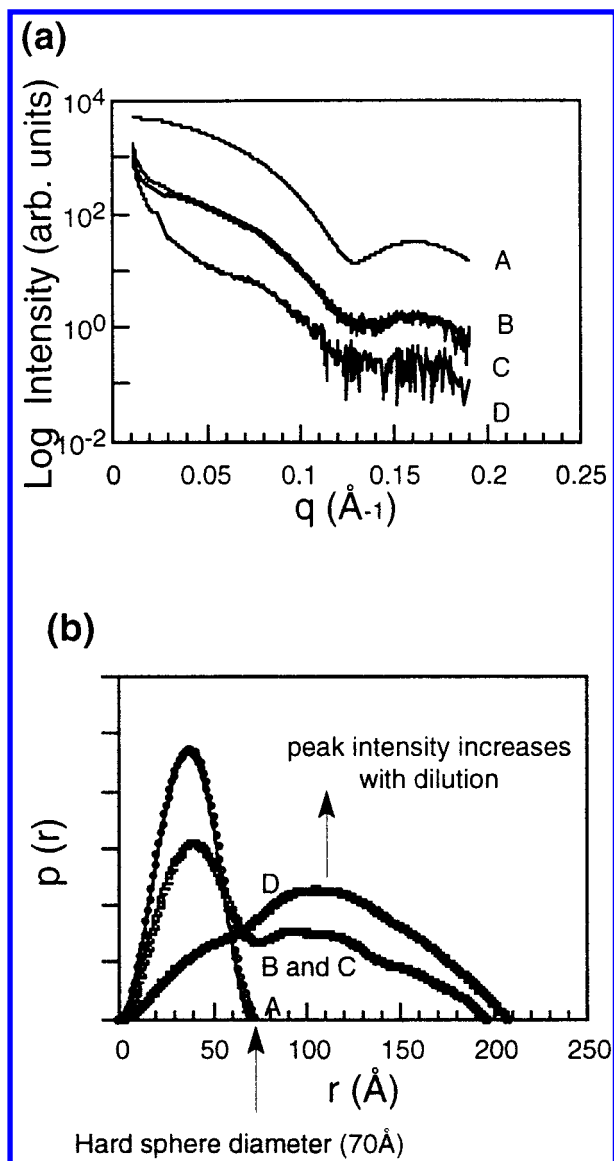
(a)

(b)

Figure 8. (a) Effect of the concentration on the angular dependence of scattered X-rays from the sample in Figure 4 (also sample (iii) in Figure 5). The curves correspond to (A) 7 mg/mL; (B) 1 mg/mL; (C) 0.1 mg/mL; and (D) 0.01 mg/mL. The increase in the relative intensity of scattered radiation at low angles from diluted samples indicates an interparticle attraction. (b) The distance distribution function, $p(r)$, calculated from the scattering data in (a). As described in the text, $p_{HS}(r)$ for a hard sphere with $R = 35$ Å is plotted and agrees with the undiluted sample. The results in (b) reveal increased reversible aggregation at higher dilutions.

the hard sphere distance distribution function, $p_{HS}(r)$,[54]

$$p_{HS}(r) = 12\left(\frac{r}{D}\right)^2\left[2 - 3\left(\frac{r}{D}\right) + \left(\frac{r}{D}\right)^3\right] \quad (8)$$

plotted in Figure 8b for a particle diameter, D, of 70 Å.) This sample is dilute (7 mg/mL corresponds to a volume fraction of 0.1%) and interparticle scattering effects ($S(q) \neq 1$) are not expected.[47] Unexpectedly, however, further dilutions increase the relative scattering at low q as seen in Figure 8a, indicating the occurrence of interparticle attraction. The corresponding plots of $p(r)$ in Figure 8b clearly show that aggregation has increased with further dilutions. Yet the scattering behavior at high q in Figure 8b remains characteristic of individual 70 Å diameter spheres. This indicates that although the interparticle attraction has increased in very dilute nanocrystal dispersions,

the corresponding aggregation remains reversible. The absence of fractal-like agglomerates in the TEM images in Figure 7 further supports this conclusion.[55]

The increased interparticle attraction in very dilute nanocrystal dispersions presumably arises from thiol desorption in the absence of free chains in the solvent resulting from the dynamic equilibrium present between adsorbed and free thiol. In this context, elemental analysis reveals that only 11% of the dodecanethiol molecules added to a typical preparation attach to the nanocrystals. The stability of the dispersion decreases significantly after it is washed, and dilute dispersions have also been found to be much less stable than very concentrated dispersions. Furthermore, polar solvents have been found to strip the adsorbed thiols from the particle surface and care must always be taken to avoid "overwashing". With increased dilution, the concentration driving force for desorption increases. As capping ligands desorb, the steric stability of the nanocrystals decreases and the propensity for particle aggregation increases.

(iii) Ellipsoidal Nanocrystals. Ellipsoidal nanocrystals form distorted hcp monolayers. In the center of Figure 9a, ellipsoidal dodecanethiol-capped silver nanocrystals with an aspect ratio of 1.3 have ordered into a distorted hcp array—or smectic-like phase—in which the particles have aligned with their long axes parallel to each other. This orientation maximizes both the vdW attraction between particles, and minimizes the nanocrystal excluded volume (translational entropy).[56,57]

In the surrounding region in Figures 9a and b, ellipsoidal particles have fused unidirectionally to form wires.[57] Nanocrystal fusion occurs when the capping ligand surface coverage is not sufficient to prevent particle surfaces from touching. Silver nanocrystals are particularly sensitive to fusion because very strong metallic bonding occurs when the interparticle separation is less than 5 Å.[46] Therefore, slight decreases in capping ligand coverage—although maybe not sufficient to induce aggregation in solution—can result in particle fusion in the monolayer when the solvent evaporates. As discussed above, the capping ligands, although chemisorbed, form relatively labile bonds with the particle surface and a driving force for both adsorption and desorption exists. Consequently, the polar solvent used for size selective precipitation strips a percentage of the capping ligands off the nanocrystal surface. Size selective precipitation therefore can be used to isolate ellipsoidal particles with aspect ratios greater than 1.3 and to slightly reduce capping ligand coverage on the nanocrystals to obtain silver nanowire arrays such as that shown in Figure 9b. These wires are as thick as the long axis of the nanocrystal (~70 Å) and are separated by approximately 15 Å by the remaining adsorbed thiolate molecules. If the particle shape is not sufficiently ellipsoidal, nanocrystal fusion occurs isotropically, as has happened in a small section of the array in Figure 9b. These wire arrays are far different than the structures expected to be formed by soft spheres.

Conclusions

Size selective precipitation effectively isolates nanocrystal dispersions that differ in average particle radius by the thickness of one lattice plane. A size distribution of the isolated dispersion nonetheless still exists; however, it is sufficiently narrow to permit long-range ordering of close-packed nanocrystal arrays as confirmed using TEM and SAXS.

FTIR and NMR spectra of the silver nanocrystal dispersion reveal the liquidlike nature of the adsorbed alkane chains extending from the nanocrystal surface into the solvent because of the extreme curvature of the particle surface. Elemental analysis confirms close-packing of the capping ligand thiol
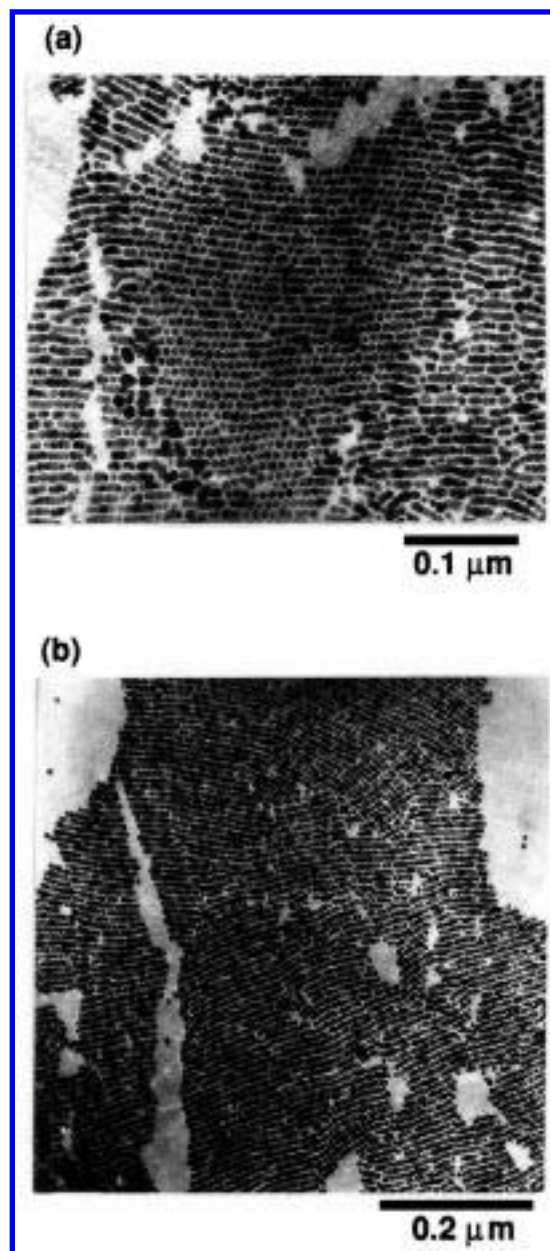
Ordered "Soft Spheres"

J. Phys. Chem. B, Vol. 102, No. 43, 1998 **8387**

Figure 9. (a) TEM image of ellipsoidal silver nanocrystals with an aspect ratio of 1.4 displaying the boundary between the distorted hcp and nanowire phases. (b) Low resolution TEM image of a silver nanowire array (average wire thickness and separation is 70 and 15 Å, respectively) formed by evaporating the solvent from a chloroform dodecanethiol-capped nanocrystal dispersion on a carbon substrate. Wire formation requires size-monodisperse nanocrystals with an aspect ratio greater than 1.3 and less than complete capping ligand surface coverage.

steric repulsion, eq 2) becomes infinitely repulsive. This corresponds to the effective soft sphere diameter.

Deviations from soft sphere behavior, however, are apparent in many instances. Although SAXS measurements of relatively concentrated dispersions of dodecanethiol-capped silver nanocrystals indicate noninteracting hard spheres, using the compositional information acquired for the capping ligands to calculate the steric repulsion between nanocrystals, a weak attractive energy minimum in the interparticle potential exists due to the strong polarizability of the metallic core. Registry between nanocrystal facets also occurs in the hcp monolayers and dilute bilayers because of the resulting anisotropic attraction between metallic cores. Very dilute nanocrystals exhibit a strong attraction because of (it is suggested) the dynamic equilibrium between bound and free thiol ligands in the nanocrystal dispersion. In addition, ellipsoidal nanocrystal cores induce the formation of distorted hcp monolayers and smectic-like phases, and in some instances, silver nanowires.

In conclusion, these nanocrystals behave essentially as soft spheres consisting of a metallic core with an organic corona. The cooperative effect of entropy at high particle volume fractions results in the extended positioning of nanocrystals at the lattice sites of an fcc supercrystal as evidenced by SAXS measurements. The highly polarizable nanocrystal core, however, induces an attraction which can affect nanocrystal orientation in condensed phases, particularly dilute ones. In addition, because of the nondeformability of the core, ellipsoidal particles can be obtained which add an additional shape-sensitive component to the phase behavior of the nanocrystals. It is expected that this fundamental framework for nanocrystal superlattice formation will aid the development of more sophisticated nanocrystal self-organization scenarios, such as cases involving two types of particles, different chain lengths of capping ligands, different particle shapes, or different substrates.

headgroups with approximately 75% coverage of surface silver atoms. FTIR spectra of the corresponding silver superlattice reveal condensed, solidlike capping ligand chains. These chains fill the void volume between silver cores in the superlattice and thus, the density of the chains determines the interparticle spacing.

The silver core volume fraction of dodecanethiol-capped nanocrystals in the superlattice is less than the particle volume fraction required to achieve entropically driven ordering of hard spheres. This implies that the particles order in a manner similar to that of soft spheres with an effective radius that includes a portion of the extended capping ligands. The final interparticle separation corresponds to the point at which the interparticle potential (calculated by summing the vdW attraction, eq 1, and

References and Notes

(1) (a) Berry, C. R. *Phys. Rev.* **1967**, *161*, 848. (b) Kubo, R.; Kawabata, A.; Kobayashi, S. *Annu. Rev. Mater. Sci.* **1984**, *14*, 49. (c) Brus, L. E. *J. Phys. Chem.* **1986**, *90*, 2555.

(2) For recent reviews, see (a) Alivisatos, A. P. *Science* **1996**, *271*, 933. (b) Schmid, G. *Chem. Rev.* **1992**, *92*, 1709. (c) Schi, J.; Gider, S.; Awschalom, D. D. *Science* **1996**, *271*, 937.

(3) Murray, C. B.; Norris, D. J.; Bawendi, M. G. *J. Am. Chem. Soc.* **1993**, *115*, 8706−8715.

(4) Herron, N.; Calbrese, J. C.; Farneth, W. E.; Wang, Y. *Science* **1993**, *259*, 1426.

(5) Vossmeyer, T.; Katsikas, L.; Giersig, M.; Popovic, I. G.; Diesner, K.; Chemsiddine, A.; Eychmüller, A.; Weller, H. *J. Phys. Chem.* **1994**, *98*, 4109.

(6) Andres, R. P.; Bein, T.; Dorogi, M.; Feng, S.; Henderson, J. I.; Kubiak, C. P.; Mahoney, W.; Osifchin, R. G.; Reifenberger, R. *Science* **1996**, *272*, 1323.

(7) Feldheim, D. L.; Grabar, K. C.; Natan, M. J.; Mallouk, T. E. *J. Am. Chem. Soc.* **1996**, *118*, 7640.

(8) Korgel, B. A.; Monbouquette, H. G. *J. Phys. Chem.* **1996**, *100*, 346.

(9) Korgel, B. A.; Monbouquette, H. G. *J. Phys. Chem. B* **1997**, *101*, 5010.

(10) Ingram, R. S.; Hostetler, M. J.; Murray, R. W.; Schaaff, T. G.; Khoury, J. T.; Whetten, R. L.; Bigioni, T. P.; Guthrie, D. K.; First, P. N. *J. Am. Chem. Soc.* **1997**, *119*, 9279.

(11) Schaaff, T. G.; Shafigullin, M. N.; Khoury, J. T.; Vezmar, I.; Whetten, R. L.; Cullen, W. G.; First, P. N.; Gutiérrez-Wing, C.; Ascensio, J.; Jose-Yacamán, M. J. *J. Phys. Chem. B* **1997**, *101*, 7885.

(12) Steigerwald, M. L.; Alivisatos, A. P.; Gibson, J. M.; Harris, T. D.; Kortan, R.; Muller, A. J.; Thayer, A. M.; Duncan, T. M.; Douglass, D. C.; Brus, L. E. *J. Am. Chem. Soc.* **1988**, *110*, 3046.

(13) See for example, Reed, M. *Sci. Am.* **1993**, *268*, 118.

(14) Roychowdhury, V. P.; Janes, D. B.; Bandyopadhyay, S.; Wang, X. *IEEE Trans. Electron Devices* **1996**, *43*, 1688.

(15) Hagfeldt, A.; Grätzel, M. *Chem. Rev.* **1995**, *95*, 49−68.

(16) Colvin, V. L.; Schlamp, M. C.; Alivastos, A. P. *Nature* **1994**, *370*, 354.

(17) Andres, R. P.; Bielefeld, J. D.; Henderson, J. I.; Janes, D. B.; Kolagunta, V. R.; Kubiak, C. P.; Mahoney, W. J.; Osifchin, R. G. *Science* **1996**, *273*, 1690−1693.

(18) Kagan, C. R.; Murray, C. B.; Nirmal, M.; Bawendi, M. G. *Phys. Rev. Lett.* **1996**, *76*, 1517.

(19) Bentzon, M. D.; van Wonterghem, J.; Morup, S.; Tholen, A.; Koch, C. J. W. *Philos. Mag. B* **1989**, *60*, 169−178.

(20) Murray, C. B.; Kagan, C. R.; Bawendi, M. G. *Science* **1995**, *270*, 1335−1337.

(21) Harfenist, S. A.; Wang, Z. L.; Alvarez, M. M.; Vezmar, I.; Whetten, R. L. *J. Phys. Chem.* **1996**, *100*, 13904−13910.

(22) (a) Motte, L.; Billoudet, F.; Lacaze, E.; Douin, J.; Pileni, M. P. *J. Phys. Chem. B* **1997**, *101*, 138−144.

(23) Collier, C. P.; Saykally, R. J.; Shiang, J. J.; Henrichs, S. E.; Heath, J. R. *Science* **1998**, *277*, 1978−1981.

(24) Kagan, C. R.; Murray, C. B.; Bawendi, M. G. *Phys. Rev. B* **1996**, *54*, 8633−8643.

(25) Alder, B. J.; Wainwright, T. E. *J. Chem. Phys.* **1957**, *27*, 1208.

(26) Alder, B. J.; Hoover, W. G.; Young, D. A. *J. Chem. Phys.* **1968**, *49*, 3688−3696.

(27) Pusey, P. N.; van Megen, W. *Nature* **1986**, *320*, 340.

(28) For equilibrium to occur at high substrate loadings, the ratio of the particle diffusion and solvent evaporation rates must be close to 1. Assuming steady-state diffusion, the characteristic time, τ, for evaporation of a solvent film of thickness, Δx, is $\tau = (\rho l \Delta x)/(D_s \Delta c)$, where ρ is the solvent density (1.483 g/cm^3 for chloroform); Δc is the concentration gradient in the gas phase (9.4×10^{-4} g/cm^3 for chloroform at 20 °C); D_s is the diffusion coefficient of chloroform vapor in air ($\sim$0.2 cm^2/sec); and l is the stagnant diffusion film thickness ($\sim$0.2 μm). When $\Delta x = 200$ Å, $\tau = 0.3$ μs for chloroform at 20 °C. The penetration distance (or diffusion length) is $x = (4\pi D_p \tau)^{1/2}$, where D_p is the particle diffusion coefficient. Using the Stokes−Einstein equation—$D_p = kT/6\pi\mu R$—to calculate D_p, a 100 Å diameter nanocrystal diffuses 100 Å after $\tau = 0.3$ μs, or one particle diameter. Because $x \propto 1/R^{1/2}$, $x/\Delta x$ is larger for smaller particles, and equilibrium is more easily achieved during solvent evaporation.

(29) The Langmuir−Blodgett phase behavior of silver and gold particles was reported recently by Heath, J. R.; Knobler, C. M.; Leff, D. V. *J. Phys. Chem. B* **1997**, *101*, 189.

(30) SAXS data showing that pyridine was a less effective capping ligand than trioctylphosphine on CdSe nanocrystals have been presented by Mattoussi, H.; Cumming, A. W.; Murray, C. B.; Bawendi, M. G.; Ober, R. *J. Chem. Phys.* **1996**, *105*, 9890.

(31) Ohara, P. C.; Leff, D. V.; Heath, J. R.; Gelbart, W. M. *Phys. Rev. Lett.* **1995**, *75*, 3466−3469.

(32) Korgel, B. A.; Fitzmaurice, D. *Phys. Rev. Lett.* **1998**, *80*, 3531−3534.

(33) Brust, M.; Walker, M.; Bethell, D.; Schiffrin, D. J.; Whyman, R. *J. Chem. Soc, Chem. Commun.* **1994**, 801.

(34) Terrill, R. H.; Postlethwaite, A.; Chen, C.-h.; Poon, C.-D.; Terzis, A.; Chen, A.; Hutchison, J. E.; Clark, M. R.; Wignall, G.; Londono, J. D.; Superfine, R.; Falvo, M.; Johnson, C. S.; Samulski, E. T.; Murray, R. W. *J. Am. Chem. Soc.* **1995**, *117*, 12537.

(35) Badia, A.; Singh, S.; Demers, L.; Cuccia, L.; Brown, G. R.; Lennox, R. B. *Chem. Eur. J.* **1996**, *2*, 359.

(36) Ulman, A. *An introduction to ultrathin organic films: from Langmuir−Blodgett to self-assembly*; Academic Press: Boston, 1991.

(37) Porter, M. D.; Bright, T. B.; Allara, D. L.; Chidsey, C. E. D. *J. Am. Chem. Soc.* **1987**, *109*, 3559.

(38) Using a shell approximation, the number of silver atoms per particle, N_{Ag}, was calculated using the relation $N_{Ag} = (\pi/6)(R_p^3/a_{Ag}^3)$ where a_{Ag} is the lattice constant for silver, 4.81 Å: Lippens, P. E.; Lannoo, M. *Phys. Rev. B* **1989**, *39*, 10935.

(39) The thickness of the outer layer of silver atoms was determined by subtracting the size of a particle with an "even" number of shells, from a particle with an "odd" number of shells.[38] The shell thickness for silver nanocrystals is 1.3 Å.

(40) Rovida, G.; Pratesi, F. *Surf. Sci.* **1981**, *104*, 609.

(41) Sellers, H.; Ulman, A.; Shnidman, Y.; Eilers, J. E. *J. Am. Chem. Soc.* **1993**, *115*, 9389−9401.

(42) Ulman, A. *J. Mater. Ed.* **1989**, *11*, 205.

(43) Using the Derjaguin approximation[44] for expressions derived in de Gennes, *C. R. Acad. Sci. (Paris)* **1985**, *300*, 839; de Gennes, C. *Adv. Coll. Int. Sci.* **1987**, *27*, 189.

(44) Derjaguin, B. V. *Kol. Z.* **1934**, *69*, 155−164.

(45) Hamaker, H. C. *Physica IV* **1937**, 1058−1072.

(46) Israelachvili, J. N. *Intermolecular and Surface Forces,* 2nd ed.; Academic Press: New York, 1992.

(47) Glatter, O.; Kratky, O., Eds. *Small-Angle X-ray Scattering*; Academic Press: New York, 1982.

(48) Kerker, M. *The Scattering of Light and Other Electromagnetic Radiation*; Academic Press: New York, 1969.

(49) McConnell, G. A.; Gast, A. P. *Phys. Rev. E* **1996**, *54*, 5447.

(50) Cohen, M. L. In *II−VI Semiconducting Compounds*; D. G. Thomas, Ed.; W. A. Benjamin: New York, 1967; p 462.

(51) An isolated dodecanethiol-capped gold nanocrystal (also assumed to be a truncated icosahedra) has also been predicted to orient on the edge between the {111} planes due to the maximization of the vdW interactions of the adsorbed chains with the substrate: Leudtke, W. D.; Landman, U. *J. Phys. Chem.* **1996**, *100*, 13323.

(52) In fact, it is the attractive potential between the particles themselves and with the substrate that results in preferential monolayer formation. As derived in detail by Korgel and Fitzmaurice,[32] an ordered nanocrystal film conceptually resembles a thin wetting film on a substrate in which the dimensionless film thickness, e/a, depends on a spreading coefficient, S, and the interaction between nanocrystals in solution, $\gamma_{nan, nan}$: $e/a = (3\gamma_{nan, nan}/2S)^{1/2}$ where S measures the relative energetic interaction between the particles and the substrate and the particles themselves, with $S > 0$ for strong interactions with the substrate. $\gamma_{nan, nan}$ describes the interparticle attraction. For dodecanethiol-capped silver nanocrystals in a good solvent on a carbon substrate, $S > \gamma_{nan, nan}$ largely because the substrate is flat and particles are spheroidal, and because the separation between the particles and the substrate ($\sim\bar{\delta}_{SL}/2$) is smaller than the interparticle separation ($\bar{\delta}_{SL}$). Therefore, these nanocrystals prefer to form monolayers because of the attractions in the system.

(53) Zernicke, F.; Prins J. A. *Z. Phys.* **1927**, *41*, 184.

(54) Porod, G. *Acta Phys. Austriaca* **1948**, *2*, 255.

(55) Fractal agglomerates form because the interparticle sticking energy is infinite: Witten, T. A.; Sander, L. M. *Phys. Rev. Lett.* **1981**, *47*, 1400.

(56) For example, the nematic phase for rodlike colloids with infinite aspect ratios results from excluded volume effects (the maximization of the translational entropy): Onsager, L. *Ann. N. Y. Acad. Sci.* **1949**, *51*, 627.

(57) For a more in-depth discussion about nanowire formation see Korgel, B. A.; Fitzmaurice, D. *Adv. Mater.* **1998**, *10*, 661−665.